Ex vivo and computer model study on retinal thermal laser-induced damage in the visible wavelength range

Karl Schulmeister
Johannes Husinsky
Bernhard Seiser
Florian Edthofer
Austrian Research Centers GmbH
Laser and Optical Radiation Test House
A-2444 Seibersdorf, Austria

Beate Fekete
Letizia Farmer
Austrian Research Centers GmbH
Toxicology Department
A-2444 Seibersdorf, Austria

David J. Lund
U.S. Army Medical Research Detachment
Walter Reed Army Institute of Research
7965 Dave Erwin Drive
Brooks City-Base, Texas 78235-5108

Abstract. Excised bovine eyes are used as models for threshold determination of 532-nm laser-induced thermal damage of the retina in the pulse duration regime of 100 μs to 2 s for varying laser spot size diameters. The thresholds as determined by fluorescence viability staining compare well with the prediction of an extended Thompson-Gerstman computer model. Both models compare well with published Rhesus monkey threshold data. A previously unknown variation of the spot size dependence is seen for different pulse durations, which allows for a more complete understanding of the retinal thermal damage. Current International Commission on Nonionized Radiation Protection (ICNIRP), American National Standards Institute (ANS), and International Electromechanical Commission (IEC) laser and incoherent optical radiation exposure limits can be increased for extended sources for pulsed exposures. We conclude that the damage mechanism at threshold detected at 24 and 1 h for the nonhuman primate model is retinal pigment epithelium (RPE) cell damage and not thermal coagulation of the sensory retina. This work validates the bovine *ex vivo* and computer models for prediction of thresholds of thermally induced damage in the time domain of 10 μs to 2 s, which provides the basis for safety analysis of more complicated retinal exposure scenarios such as repetitive pulses, nonconstant retinal irradiance profiles, and scanned exposure. [DOI: 10.1117/1.2982526]

Keywords: laser safety; retinal thermal damage; damage threshold; computer model; ANSI Z136.1; IEC 60825-1.

Paper 07408R received Sep. 28, 2007; revised manuscript received Jun. 7, 2008; accepted for publication Jun. 10, 2008; published online Sep. 23, 2008.

1 Introduction

Intense optical radiation can induce temperatures in the retina that are high enough to cause injury. Such thermally induced retinal damage is typically associated with laser radiation, but can also be induced by intense broadband radiation. We discuss laser-induced thermal damage; however, the discussion regarding spot size dependence and pulse duration dependence also directly applies to broadband radiation. Exposure limits (EL) for laser radiation and incoherent broadband optical radiation are set on the international level by the International Commission on Nonionizing Radiation Protection (ICNIRP),[1,2] but are also adopted by standards committees and are also referred to as maximum permissible exposure (MPE).[3–5] The basis of current exposure limits are experimental animal injury threshold data. Nonhuman primates (NHP), especially the rhesus monkey, have so far been the model of choice for determining laser-induced retinal injury threshold values that underlie retinal exposure limits. Most threshold data were obtained for exposure to a collimated beam, which produced the minimal image diameter at the retina. The current dependence of retinal thermal laser exposure limits on retinal spot size is discussed in Henderson and Schulmeister.[6]

Mathematical thermal damage models, such as the "Takata model",[7] or the Thompson-Gerstman model,[8] have not yet been applied to study the spot size dependence for the full range of applicable pulse durations. The collection of experimental data related to the retinal image diameter dependence of threshold laser-induced thermal retinal injury is relatively limited and was reviewed by Lund et al.[9] We report on the results of laser exposure of a bovine *ex vivo* (explant) model and of computer models that were validated by comparison with NHP injury threshold data. The models appropriately predict absolute damage threshold values in the visible wavelength range for exposure durations from 10 μs to 2 s. The data provide an understanding of the spot size dependence of retinal thermal injury thresholds in the visible wavelength range, which can be the basis for improving the accuracy of both laser and broadband retinal thermal MPEs.

We present retinal injury threshold data both in terms of the total intraocular energy (TIE), and in terms of retinal

Address all correspondence to Karl Schulmeister, Laser and Optical Radiation Test House, Austrian Research Centers, A-2444 Seibersdorf, Austria. Tel: +43–50550–2533; E-mail: karl.schulmeister@arcs.ac.at

1083-3668/2008/13(5)/054038/13/$25.00 © 2008 SPIE

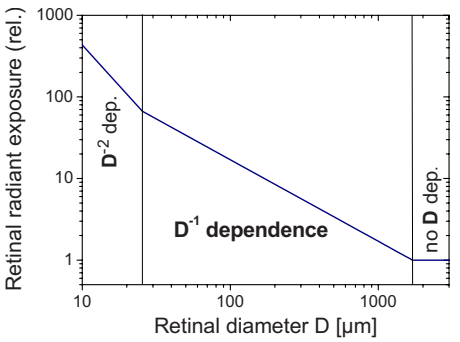

(a)

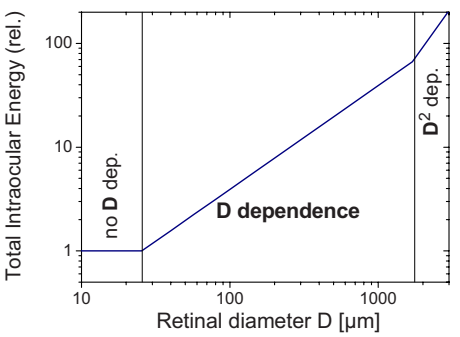

(b)

Fig. 1 (a) General dependence of the current MPE values (specified as corneal levels) as a function of the retinal spot diameter D (b) General dependence of the current MPE values when specified as retinal radiant exposure.

radiant exposure. The energy per pulse that is incident on the retina can be calculated by multiplying the TIE with the transmittance of the ocular media in front of the retina. For a constant irradiance profile (top-hat profile), the retinal radiant exposure in units of J cm^{-2} can be calculated from this value by division with the area over which the energy that is incident on the retina is distributed. When D is the diameter of the laser spot on the retina, then the retinal radiant exposure H_{ret} is directly proportional to TIE D^{-2}. With these relationships, it is possible to discuss the spot size dependence of the retinal thermal injury thresholds in retinal space by analyzing the damage threshold in terms of retinal radiant exposure (with units of J cm^{-2}) or in corneal space, where the threshold for retinal damage is specified in terms of the TIE (with units of J or μJ). The MPE multiplied with the area of 7-mm-diam averaging aperture can be compared to the threshold given as the TIE. The MPE multiplied with the area of 7-mm-diam averaging aperture and divided by D^2 can be compared to the threshold data given as H_{ret}. The two equivalent ways to plot the spot size dependence of the MPEs and damage threshold data are shown in Fig. 1. A linear dependence on D in corneal space will be transformed to a $1/D$ dependence when the data are plotted as retinal radiant exposure. For values of D larger than a critical value $D_{\max}$ (currently set to 100 mrad in the MPEs), the spot size dependence in terms of TIE is proportional to D^2, which will be transformed to a D^0 dependence (i.e., no dependence on D) when the data are plotted as retinal radiant exposure. It is beneficial to plot the data in terms of retinal radiant exposure [Fig. 1(a)] when discussing the general spot size dependence to see where the threshold data does not depend on the spot diameter (which would be a D^2 dependence in terms of TIE). It is beneficial to plot the data in terms of TIE [Fig. 1(b)] to show and discuss the spot size dependence in the small-spot regime to see where the data plotted as TIE does not exhibit a spot size dependence. To facilitate the comparison between different models and the human case, the retinal spot size is given in terms of diameter D (in units of μm) and not in terms of angular subtense, since the diameter is the basic quantity and the angular subtense depends on the length of the eye, which is different for the Rhesus monkey and the human (i.e., for the same angular subtense, the image on a Rhesus monkey retina is smaller than on a human retina).

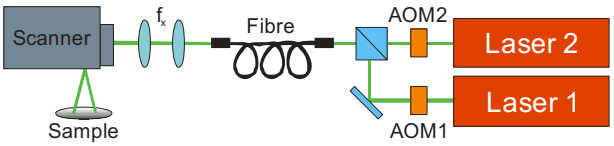

Fig. 2 Experimental setup for the *ex vivo* explant exposures.

2 Materials and Methods

2.1 *Experimental Setup*

Figure 2 shows a schematic overview of the setup for the irradiation of the samples, with the exception of minimal spot diameters. Two frequency-doubled Nd:YAG lasers (Omicron Laserage FK-LA 8000, Rodgau, Germany) provide continuous laser radiation at a wavelength of 532 nm and with a total output power of up to 18 W. These lasers have a beam propagation factor M^2 of about 8. In front of each laser aperture, a computer-controlled acousto-optical modulator (AOM1 and AOM2) was placed. The AOMs control the laser power as function of time with a temporal resolution of 10 μs and a throughput resolution of 1024 steps between zero and maximum transmission, and thus allow control of both the pulse shape as well as the energy per pulse. For the experiments reported in this work, the temporal pulse shape was rectangular. After combining the two laser beams by a polarization crystal, the beam was coupled into either a 50-μm (for spot sizes less than 1 mm) or a 200-μm fiber, (for spot sizes 1 mm or greater). A lens imaged the distal tip of the fiber onto the sample. The length of the fiber was 10 m. The beam finally enters a galvanometer-driven scan head (SCANLAB hurry *SCAN*™ 14, Puchheim, Germany), which produces a computer-controlled scan pattern on the sample. Concurrent control of the scanner and the AOMs was affected with a PC interface card (SCANLAB RTC® 4) and a self-developed computer program. With this computer program, it is possible to expose a sample with a grid of individual laser exposures in a short amount of time. For instance, for small laser spots (23 μm), it is possible to place 200 exposures with varying energy per pulse on a sample area of 5×5 mm^2 within one minute. A calibrated laser power meter [Ophir 3A and Ophir L40(150)A, North Logan, Utah] was placed beneath the scanner before and immediately after the exposures to record the power incident on the sample for an "open" AOM, i.e., the maximum peak power level. The actual energy deposited on

each irradiated location on the sample was calculated in Microsoft Excel, using pulse duration, power, and the AOM's throughput setting, which was calibrated with the laser power meter. The experimental uncertainties related to the power incident on the sample are: laser power instability less than ±3%; uncertainty of power radiometers ±3%; and deviation of AOM throughput from calibration function ±1% resulting in a total power uncertainty of ±4.4%. Prior to the exposures, the spatial beam profile was recorded in the sample plane with a COHU charge-coupled device camera (model 7512) with 6.7-μm pixel pitch, and the beam diameter defined at the 1/e level was calculated with a beam analyzer software (Spiricon LBA-700PC North Logan, Utah). The beam profile on the sample for all but the smallest laser spots was a nominal top hat, i.e., inconstant irradiance level (the difference of the threshold between a perfect top hat and the actual profile was calculated with the thermal model to be less than ±2%). To achieve small spots (23 μm diam), a continuous frequency-doubled Nd:YAG TEM_{00} laser (CrystaLaser GCL-100-L, Reno, Nevada) with a wavelength of 532 nm and 100-mW output power was used instead of the two Omicron lasers. This laser has a M^2 value of close to 1 and the beam profile for the 23-μm-diam spots (diameter specified at the 1/e level) was Gaussian. For the 23-μm spots, no fiber was used. The uncertainty of the diameter measurement for the 23-μm spots was estimated to be ±14%, for 73-μm spot size ±5%, and for the larger spot sizes less than ±3%.

2.2 *Sample Preparation and Analysis*

The *ex vivo* (explant) samples were obtained from fresh bovine eyes that were received from a local slaughterhouse. After dissection of the surrounding connective tissue, the eye was opened approximately 7 mm beneath its equator and the vitreous body was removed. The black-pigmented parts of the fundus of the eye were cut into rectangular pieces and placed in phosphate-buffered solution. The sensory retina (the photoreceptor layer and attached nerve layers) was removed by cleaving the outer segments of the photoreceptors with Chondroitinase ABC (Sigma-Aldrich, Missouri), so that the uppermost layer was the retinal pigment epithelium (RPE), supported by the choroid and the sclera. Then, the tissue was stained with the viability marker Calcein AM (2.5-μM/ml phosphate buffered saline, Sigma Aldrich, Missouri). Calcein is absorbed by the vital cells and reduced to a fluorescent dye by means of cellular esterases (excitation maximum at 490 nm, emission at 520 nm). The incubation time before laser exposure was between 30 min and 2 h. The samples were examined before laser exposure with a Zeiss Axiovert (Jena, Germany) inverted microscope to ensure viability of the cells and quality of the sample. Subsequent to the examination, the samples were stored in Hank's Balanced Salt Solution (Krackeler Scientific, Albany, New York). The RPE cells remained vital for a total duration of 8 to 10 h after slaughtering of the animals. The samples were also kept covered with Hank's Solution during laser exposure to prevent dehydration. The temperature of the sample before laser exposure was 23 ± 1 °C. The examination of viability with the Zeiss Axiovert inverted microscope took place between 15 min and 1 h after exposure. For some samples, the development of lesions over time was observed, and it was found that the number of cells showing damage did not increase after the 15-min postexposure evaluation. Vital cells show a bright green fluorescence, whereas the damaged cells appear dark due to loss of dye. The examination was performed by Husinsky only due to time constraints regarding the viability of the samples. A horizontal and vertical line with overexposed "shots" formed a cross in the exposure grid to aid the evaluation. Exposed sites where determined to be either damaged or not affected. It was noted that on occasion, the exposed area appeared distinctively brighter than the surrounding nonexposed area, or that highly fluorescent droplets formed at the edge of the region where cells were dark (see Fig. 3). For very small laser spots, occasionally only droplets could be seen and it was not possible to determine whether the cell behind the droplet appeared dark (i.e., dead) or fluorescent. The exact reason for this increased brightness and formation of droplets is not known but is expected to be related to leaking of Calcein out of compromised cells. These cases were also counted as damaged. The lesion dose-response data were evaluated by Probit analysis software (ProbitFit V1.0.2 by Brian Lund, Northrop Grumman, Los Angeles, California) to obtain ED50 and slope values (see for instance Sliney et al.[10] for a discussion on these parameters). A light micrograph (40× magnification) of a histological section showing the lesion confined to the RPE is shown in Fig. 4.

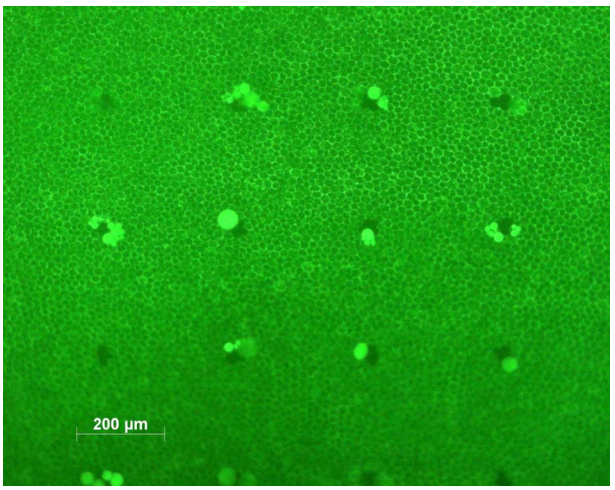

Fig. 3 Fluorescent micrograph of exposures with a beam diameter of 23 μm and a pulse duration of 100 ms. The energy per pulse was varied. Individual RPE cells are visible.

2.3 *Computer Model*

Laser-induced retinal thermal injury thresholds were calculated with a computer model based on the concept published by Thompson et al.,[8] usually referred to as the Thompson-Gerstman model. However, the basic model was extended to also model the choroid as an absorbing layer, which is necessary for accurate calculations in the thermal damage regime. The absorbing spheres in the model were regarded as means to couple radiant energy into the system and were not intended to model actual distributions of melanosomes. In the pulse duration regime of interest to thermal damage, the absorbing layers of the RPE and choroid can be treated as

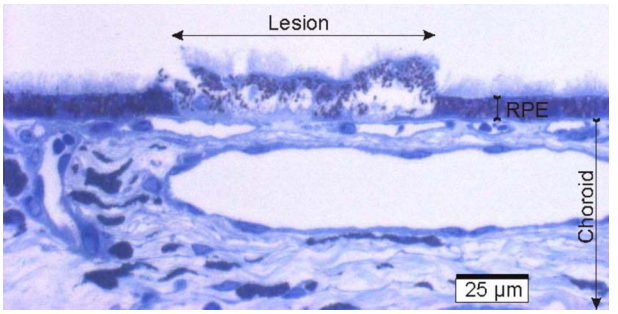

Fig. 4 Light micrograph of a histological section showing a damaged RPE layer in the center and normal RPE to both sides.

homogeneous absorbers; the localized absorption by melanosomes only plays a role for pulse durations in the microsecond regime and shorter (where, however, microbubble formation is the dominating damage mechanism, which cannot be modeled with the Thompson-Gerstman model). A comparison with a finite difference model (also often referred to as the Takata' model[7]) showed that for an equivalent percentage of absorption in the retina, the Thompson-Gerstman model for pulse durations above 10 μs yields threshold damage values identical to those calculated with the finite difference model. This equivalence is due to the homogenization of the temperature field by heat flow, which after some time averages out the hotspots around the melanosome spheres. The Thompson-Gerstman model was used for the temperature calculations presented here. The advantage of this extended Thompson-Gerstman model is that it is, in many cases, much faster than, for instance, a model based on finite differences or finite elements. To avoid variabilities due to the placement of the laser spot on the computational grid, a regular distribution of melanosomes was chosen. No shadowing was assumed in the RPE, i.e., the irradiance level as a function of depth was constant. The RPE thickness (or rather, the thickness of the high-pigment-density layer in the RPE) was set to 5 μm. The melanosome diameter was 0.8 μm, melanosome spacing (center to center) was 1 μm, and the absorption coefficient of the melanosome was set to 4609 cm^{-1}, which resulted in an absorptance of 67% in the RPE and an equivalent homogeneous bulk absorption coefficient of 1340 cm^{-1}. The absorption coefficient of the RPE was varied to find the value that would provide an optimum fit to the explant *ex vivo* damage threshold data for the complete range of pulse durations (0.1 ms to 2 s) and spot diameters (23 μm to 2 mm). The choroid was populated with melanosomes with 1 μm diam, placed next to each other, with an absorption coefficient of 36 cm^{-1} and an exponentially decreasing irradiance level with an effective absorption coefficient of 150 cm^{-1}. This value is specified for Negro by Takata et al..[7] The choroid was assumed to be thick enough so that the thickness would not influence the calculated thresholds, i.e., the choroid is assumed to be semi-infinite. Thermal properties of water at 65 °C were used for all media,[11] i.e., a density of 1 g cm^{-3}, specific heat of 4.185 J g^{-1} K^{-1}, and thermal conductivity of 0.00629 W cm^{-1} K^{-1}. It is necessary for the Thompson-Gerstman model to assume that all media within the model have the same thermal properties and that these are constant with time. Consequently, varying thermal properties in different layers or temperature dependent values cannot be modeled. The Arrhenius integral was used to calculate damage thresholds, and the rate and energy parameters were chosen as given by Welch and Polhamus,[12] i.e., $A=1.3\ 10^{99}\ s^{-1}$ and $E/R=75519$ K. The minimum retinal area, which had to reach an Arrhenius integral value of at least 1 to be recorded as damaged, was set to a diameter of 20 μm. The model parameters described in this section were used without adjustment or variation to model the complete range of experimental threshold parameters of pulse durations from 10 μs to 2 s and spot sizes between 23 μm and 3 mm, including both Gaussian as well as top-hat irradiance profiles.

3 Results

3.1 *Ex Vivo Bovine and Computer Model*

The explant *ex vivo* damage thresholds (ED50) of this study are summarized in Table 1 and are shown in Fig. 5 together with results of the extended Thompson-Gerstman computer model. The overall variability and uncertainty for the ED50 values is estimated to be about ±20%. The explant *ex vivo* thresholds cover a pulse duration range of 100 μs to 2 s and a spot diameter range of 23 μm to 2 mm. The computer model data were extended to include also values for 10-μs pulse duration and spot sizes of up to 3 mm. The slope *S* (ED84/ED50) that results from Probit analysis of the experimental data is close to 1 (typically less than 1.1, but never larger than 1.2), indicating both little variability within different eyes as well as a small uncertainty.[10] When the slope is listed as <1.01, the probit analysis software indicated that the value of the slope was so close to 1 that the calculated slope (less than 1.01) was somewhat uncertain. To derive the 31 threshold injury values, a total number of 4911 exposures were placed on 166 retinal samples. These numbers underpin why it is not realistic to obtain a full set of threshold data in terms of pulse duration and spot size dependence with *in vivo* models.

Two regions can be clearly distinguished in Fig. 5, one where the logarithmic slopes of the threshold curves (threshold as function of diameter *D*) are close to −1, i.e., a $1/D$ dependence, and another where the thresholds do not depend on the diameter *D*, i.e., a logarithmic slope of 0. These two regions are separated by an inflection point in the curve. The position of the inflection point depends on the pulse duration: the longer the pulse duration, the larger the spot size value where the inflection occurs. The computer model data fit the experimental data over the full range of retinal spot diameters and pulse duration to within a factor of better than 1.2. For retinal spot diameters less than about 30 μm, both the computer model and the experimental threshold data exhibit a spot size dependence that is steeper than −1.

The threshold data can also be plotted as function of pulse duration for a given spot size (Fig. 6). The pulse duration dependence data shown in Fig. 6 can be envisaged as a vertical section through the spot diameter dependence data of Fig. 5: for small spots, in Fig. 5, the lines for given pulse durations are spaced a farther apart than for large spot diameters. This represents a different pulse duration dependence of the thresholds for small and large spot diameters, which can

Table 1 Probit threshold data for the range of pulse durations between 100 μs and 2 s and retinal spot diameters, where relevant, from 23 μm to 2 mm for the bovine *ex vivo* explant model for 532-nm laser radiation. The Slope *S* is defined as ED84/ED16, and FL stands for fiducial limits. The profile for 23-μm-diam retinal spots was Gaussian (1/e diameter criteria): all larger spots were constant-irradiance profile (top hat). The ED50 given as retinal radiant exposure was determined from the ED50 given in terms of total energy (TIE) by division with the area calculated from the spot diameter.

Pulse duration [ms]	Spot diam [μm]	ED50 [μJ]	ED50 [J cm^{-2}]	Lower FL [J cm^{-2}]	Upper FL [J cm^{-2}]	Slope S	Number of samples	Number of exposures
0.1	73	12	0.29	0.29	0.30	1.02	4	100
	120	32	0.28	0.28	0.29	1.04	10	250
	288	196	0.30	0.29	0.31	1.03	5	180
1	23	8	2.03	1.95	2.11	1.06	1	147
	73	30	0.72	0.70	0.74	1.04	2	50
	120	85	0.75	0.73	0.77	1.07	10	250
	288	456	0.70	0.65	0.74	1.05	3	214
	549	1685	0.71	0.71	0.71	<1.01	1	9
10	23	46	11.13	10.72	11.52	1.11	1	196
	73	147	3.51	3.42	3.61	1.16	3	588
	120	241	2.13	2.04	2.22	1.10	3	196
	288	1212	1.86	1.69	2.01	1.15	2	72
	549	4740	2.00	2.00	2.00	1.04	4	36
	894	9766	1.56	1.56	1.56	1.09	3	16
	1508	28991	1.62	1.62	1.62	1.03	11	44
100	23	376	90.41	87.46	93.31	1.03	1	196
	73	808	19.30	18.70	19.88	1.01	3	75
	120	1362	12.04	11.74	12.34	1.02	5	196
	288	4062	6.23	6.23	6.23	1.01	2	36
	549	10968	4.63	4.63	4.63	1.01	2	18
	849	28260	4.50	4.50	4.50	<1.01	5	20
	1508	72276	4.05	4.05	4.05	<1.01	9	32
655	23	1824	439.03	420.17	457.55	1.12	4	196
	73	4907	117.23	112.63	121.73	1.09	3	196
	120	7779	68.78	67.45	69.68	1.05	9	909
	288	16203	24.87	22.88	26.69	1.19	3	90
	894	69367	11.05	8.79	12.29	1.14	8	32
	2000	273788	8.71	6.49	9.75	1.08	6	24
2000	120	21104	186.60	183.05	190.07	1.06	11	350
	549	98866	41.76	40.22	43.29	1.06	13	117
	2000	690386	21.98	21.11	22.85	1.06	19	76

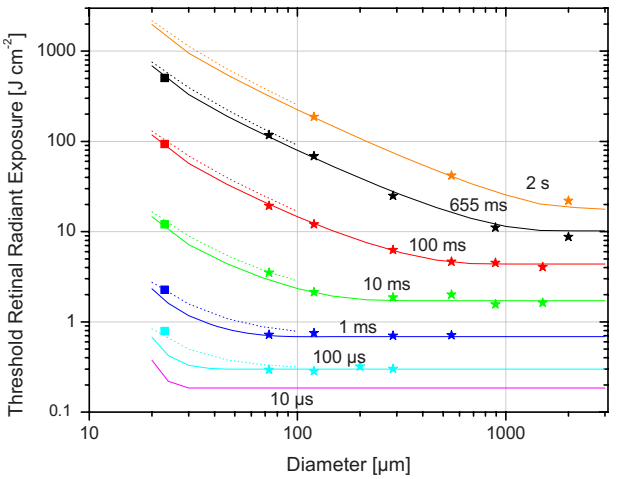

Fig. 5 Damage threshold values for bovine explant *ex vivo* samples plotted as retinal radial exposure as a function of retinal spot diameter. Square symbols indicate a Gaussian beam profile (small spots), and star symbols represent top-hat profiles. The lines are the result of an extended Thompson-Gerstman model, full lines indicate top hat, and dotted lines Gaussian profiles.

be seen in Fig. 6. For pulse durations below about 0.1 ms, the family of curves merge (except for the curve for 23-μm spot size, which is due to the Gaussian profile), and for pulse durations below about 10 μs, the computer model data show no pulse duration dependence, as is expected for the condition of thermal confinement. For pulse durations longer than about 0.1 ms, the family of curves separate: the curves for small spot diameters separate for shorter pulse durations, and the curves for larger spots separate only at longer pulse durations. Those curves that are separated, i.e., the small spot diameter curves, approach a pulse duration dependence with a slope of $t^{0.9}$. The large spot diameter threshold data follows a pulse duration dependence of $t^{0.41}$.

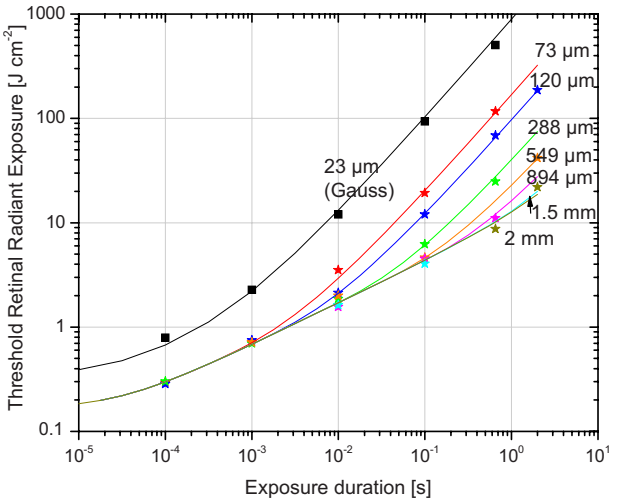

Fig. 6 *Ex vivo* and computer model threshold data shown in Fig. 5 plotted as a function of pulse duration for a range of retinal spot size diameters.

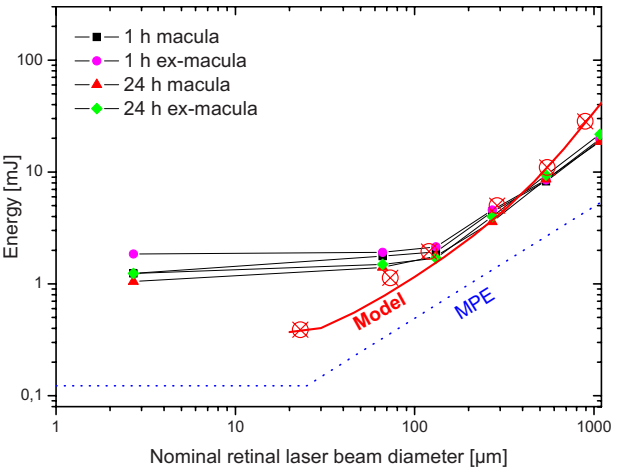

Fig. 7 100-ms NHP threshold data (small symbols), bovine *ex vivo* threshold data (large crossed circles), model data (full red line), and the current MPE values (dotted blue line). The data are plotted in terms of TIE (corneal space) (not corrected for transmission losses for the case of the NHP model). (Color online only.)

3.2 *Comparison with* 100-ms *Nonhuman Primate Threshold Data*

Recently, *in vivo* laser-induced retinal injury thresholds were determined in the Rhesus monkey for exposure to a 514-nm argon laser with a pulse duration of 100 ms for a range of retinal spot diameters,[9] as shown in Fig. 7. In Fig. 7, the nominal retinal spot diameter is not the actual diameter at the monkey retina (which is not known), but rather a theoretical value that would apply for a perfect optical system. The value of the nominal retinal laser spot diameter is derived from the measured far-field divergence of the laser beam equal to the angular subtense of the retinal image for an eye accommodated to infinity. This nominal value is to be differentiated from the actual retinal spot diameter, which might be larger due to scattering, for instance. The laser beam diameter at the cornea was 2.5 to 3 mm to minimize the influence of aberrations of the eye. The *in vivo* data (1-h and 24-h endpoint, macula and extramacula) are shown in Fig. 7 together with injury threshold data resulting from laser exposure of the bovine *ex vivo* explant and results from the computer model. In the range of spot diameters between 100 and 600 μm, the computer results and ex plant data fit very well with the NHP data, with the difference being less than a factor of 1.3. When plotted as TIE (Fig. 7), the computer and *ex vivo* data continue to decrease for spot diameters less than 100 μm, while the NHP data remains constant.

3.3 *Comparison with Nanosecond and Microsecond Data*

The current spot size dependence of the MPEs has been in doubt for some time, especially for pulse durations in the microsecond range and for shorter pulses. In the condition of thermal confinement for a homogeneous absorbing layer (i.e., when the pulse duration is shorter than the time it takes for heat flow to have an effect on the threshold), it would not be expected that the threshold in terms of retinal radiant exposure would depend on the diameter of the retinal spot, but

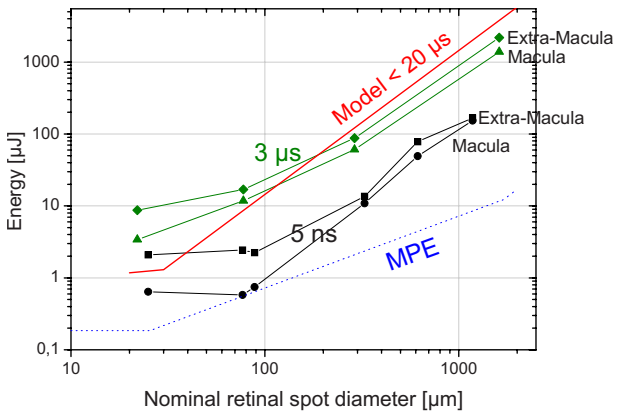

Fig. 8 Experimental 24-h retinal injury threshold values (TIE) for 3-μs-duration exposures (590 nm) and 5-ns duration exposures (532 nm) from Zuclich et al.[13] The computer model data for pulse durations less than 20 μs are also shown as a full line. Also shown are the current MPE values.

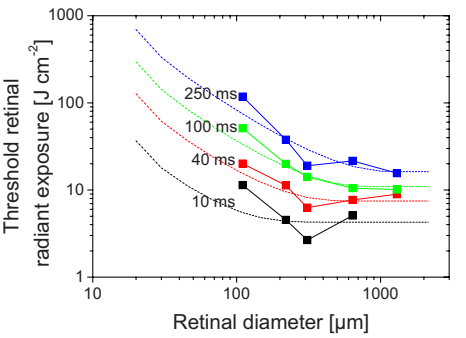

Fig. 9 NHP threshold data[18] for exposure to a xenon lamp obtained 5 min after exposure (symbols) and computer model threshold data (lines, this work) for four different pulse durations, as a function of retinal spot size. The NHP threshold data, expressed as retinal radiant exposure, are not corrected for preretinal transmission losses, i.e., the values are derived by dividing the TIE threshold value with the area of retinal exposure.

should depend only on the local radiant exposure value. This concern was supported by a study published[13] in 2000 for nanosecond and microsecond pulse durations (data shown in Fig. 8.). The NHP *in vivo* laser-induced retinal injury thresholds of that study exhibit a D^2 dependence when plotted as TIE (i.e., no spot size dependence when plotted as retinal radiant exposure) for spot sizes above about 80 μm, as would be predicted by thermal models. The threshold data, as calculated with the extended Thompson-Gerstman model used in this work for pulse durations less than 20 μs and for spot diameters above 100 μm, compare quite well with the *in vivo* injury thresholds determined for 3-μs-duration exposures, but is a factor of about 10 too high compared to injury thresholds determined for 5-ns-duration exposures. Schüle et al.[14] as well as Lee, Alt et al.[15] showed in an explant *ex vivo* model that for pulse durations less than about 10 μs, cell death induced by bubble formation around the melanosomes (microcavitation) has a lower threshold than thermally induced cell death. Thus, bubble-induced cell damage appears to be the reason for the difference between the 5-ns and 3-μs pulse duration thresholds.

The injury thresholds, when plotted as TIE as shown in Fig. 8, for spot sizes smaller than about 80 μm (for the 3-μs exposures at a less well-defined breakpoint than for the 5-ns data) do not follow this expected D^2 dependence. The 5-ns data do not exhibit any spot size dependence, and the 3-μs data show a distinctively shallower spot size dependence than the expected D^2 dependence. This "small spot—spot size behavior" has presented a challenge for interpretation and understanding since the publication of the data. A similar small spot threshold behavior is also found for millisecond-duration exposures (Fig. 7) as well as for ultrashort and seconds-duration exposures, as reviewed by Lund et al.[9] The discussion is also relevant for the problem that the damage threshold for 5-ns pulse duration and 77-μm retinal spot diameter is basically at the current MPE value, i.e., there is a need that the respective MPEs are reduced.

3.4 *Other Threshold Data*

In published *in vivo* laser-induced retinal injury threshold studies, no NHP threshold data are available where the spot size dependence in terms of the inflection point between D^{-1} threshold dependence and D^0 dependence for the retinal radiant exposure can be evaluated. In the microsecond and nanosecond pulse duration regime, the spot size dependence is already D^0 for all spot sizes greater than about 80 μm. The only available NHP threshold data for longer laser exposures is for[16,17] 250 ms and 1 s, but these threshold data do not include data for sufficiently large spot sizes, so that the data only shows the D^{-1} dependence. The only NHP retinal injury threshold data that cover a large enough spot size range in the millisecond range was obtained for xenon arc lamp exposure,[18] and these data do show the predicted breakpoint with D^{-1} dependence of the retinal radiant exposure thresholds to the left of the breakpoint and D^0 dependence for spot sizes larger than the breakpoint (Fig. 9).

All published NHP threshold data in the visible wavelength range that included at least three different spot sizes for pulse durations between 1 ms and 1 s are collected in Table 2. For each set of experimental threshold values, a multiplication factor was chosen to approximately minimize the difference between the experimental values and the computer model data. This multiplication factor for the computer model data also covers the influence of differences in retinal absorption for different wavelengths, as well as differences in tissue baseline temperature. The optical transmission was corrected for the NHP data to calculate energy incident on the retina by using the ocular transmission data of Maher.[19]

In the interpretation of the value of the multiplication factor as "goodness of fit" of the calculated data, it needs to be considered that the experimental data are influenced by a number of factors,[10] such as the region of the retina, the time of determination of the ophthalmoscopically visible lesion, and differences in ocular transmission and retinal absorption depending on wavelength. The macula is more highly pigmented, and thus macular thresholds are lower than thresholds determined in the extramacula. Some studies used a 5-min endpoint such as for the xenon arc lamp data, while others use

Table 2 Comparison of available experimental threshold data with calculated thresholds. The criteria for selection of the experimental data were: wavelength range between 400 to 700 nm, pulse duration between 1 ms and 1 s, Rhesus monkey eyes, and minimum of three data points for different spot sizes.

Author reference	Mult. Factor	Wavelength	Pulse duration	Spot size range (number of data points within that range)	Range of relative difference
Beatrice and Frisch[16]	0.8	514 nm	1 s	50 to 598 μm (3)	0.98 to 1.04
Ham et al.[17]	1.6	633 nm	250 ms	50 to 211 μm (3)	0.7 to 1.1
			1 s	50 to 325 μm (4)	0.8 to 1.3
Allen et al.[18]	0.8	694 nm	2 ms	135 to 1350 μm (4)	0.91 to 1.06
Allen et al.[18]	2.0	400 to 900-nm Xenonarc lamp	4 ms	220 to 640 μm (3)	1.5 to 2.2
			10 ms	110 to 640 μm (4)	0.5 to 1.9
			20 ms	10 μm (1)	0.5
				220 to 1300 μm (4)	0.8 to 1.2
			100 ms	110 μm (1)	0.63
				220 to 1300 μm (4)	0.90 to 1.08

a 1- or 24-h endpoint. The 24-h thresholds are typically lower than the 5-min or 1-h thresholds. Also it is noted that the temporal pulse profile will have an influence on the threshold; for the *ex vivo* explant data presented in this work, rectangular temporal pulse shapes were used, which should be representative of those studied that used cw sources and shutters to define the pulse duration. Also the retinal profile in experimental studies is often Gaussian and not top hat, as assumed in the calculations, which gives rise to a difference, depending on the pulse duration, of up to a factor of 1.4 (ongoing modeling work, to be published).

Considering the range of pulse durations (3 orders of magnitude) and the range of spot sizes from 50 to 1300 μm (i.e., per study, usually over a range of a factor of 10 from the smallest to the largest spot), the general trend in terms of spot size dependence for different pulse durations, as predicted by the thermal model, fits very well with the available experimental data. Once a corresponding multiplication factor is chosen for a given experimental study, the difference between the model and the experimental data is generally less than $\pm$30%. The spot size dependence is particularly well predicted for the 514-nm, 1-s *in vivo* data of Beatrice and Frisch,[16] where the difference is less than $\pm$4% for three spot sizes between 50 and 600 μm, as well as for the data of Allen et al.[18] for 694-nm, 2 ms-duration exposures at four spot sizes between 135 to 1350 μm, where the relative difference is less than $\pm$9%. Also most of the xenon arc lamp data of Allen et al. is very well described by the model calculations, with relative differences of less than $\pm$10% for 100-ms duration exposures at spot sizes between 220 to 1300 μm. The multiplication factor values reported in Table 2 fall well within the range, which can be expected for listed variabilities and experimental uncertainties.

4 Discussion

4.1 *Comparison with Nonhuman Primate* 100-ms *Data*

Figure 7 shows that for retinal spot sizes larger than about 80 to 100 μm, the *ex vivo* bovine thresholds agree to within a factor of 1.3 with the 24-h *in vivo* NHP threshold data (the small spot data are discussed in Sec. 4.2). It is noted that *in vivo* 1- and 24-h threshold data for extramacula and macula exposures are also very similar with each other and only differ noticeably for spot sizes less than 80 to 100 μm. The *in vivo* threshold for a diameter of 1080 μm is lower than the interpolated bovine *ex vivo* explant threshold, as seen in Fig. 7. The reason for this difference is not entirely clear but could be due to the nonperfect top-hat profile of the monkey threshold. An inner region of higher retinal irradiance could lead to a smaller effective thermal diameter, so that this threshold in terms of TIE would have to be plotted at a smaller nominal retinal diameter—for instance, if this effective thermal diameter were 750 μm, it would lie on the curve predicted by the computer and bovine model. The spot size dependence in the spot diameter range between 100 and 500 μm when plotted as retinal radiant exposure is almost exactly D^{-1}, i.e., the logarithmical slope of the threshold curve is, within the experimental uncertainly, identical to -1. Unfortunately, the monkey data currently do not include large enough spot sizes to reach up to the inflection point of the spot size dependence, as seen in the *ex vivo* bovine and computer models.

The closeness of the thresholds for the different models for spot sizes larger than 80 μm might be surprising due to the difference of the *in vivo* NHP and the *ex vivo* bovine models and endpoints. For the *ex vivo* bovine samples, the RPE cell layer is exposed directly, i.e., there is no optical loss (reflection or absorption) due to preretinal media as in the NHP eye, as well as there is no pre-RPE influence on the laser profile (such as scattering). The transmittance associated to the rhesus monkey preretinal media for 532 nm equals[19] 0.57. The inverse of 0.57 equals 1.7, and by this factor, the *in vivo* NHP TIE threshold should be higher than the *ex vivo* bovine threshold. However, the *ex vivo* bovine sample is at room temperature (23 ± 1 °C) and the monkey body temperature is about 38 °C, resulting in a lower threshold for the monkey. The computer model predicts a difference in thresholds by a factor of 1.5 for these two different background temperatures, compensating to a large degree for the difference in optical transmissivity.

More importantly for the validation of the *ex vivo* bovine model are the different endpoints. The *ex vivo* explant bovine thresholds are determined at about 15 min after exposure and they are based on RPE cell viability. *In vivo* NHP thresholds on the other hand are determined ophthalmoscopically (i.e., optical appearance change of the fundus) 1 and 24 h after exposure. From the similarity of the threshold data for spot sizes larger than 80 μm, it appears that the underlying mechanism is in both cases immediate RPE cell damage. Since the sensory retina is very weakly absorbing in the visible wavelength range (approximately 5%), for comparable pigmentation of the RPE in the two models, the temperature rise would be equivalent for the same retinal radiant exposure. It stands to reason that the RPE in the NHP model would be damaged at exposure levels similar to those that lead to RPE damage in the *ex vivo* explant model. For the case of the *in vivo* NHP threshold experiments, however, the viability of RPE cells cannot be determined, and detection of a lesion is based on a change of visual appearance, i.e., change of color or reflectance of the retina. The uppermost layer that is imaged is the sensory retina, not the RPE (outside of the fovea, the sensory retina has a thickness of about 200 to 300 μm). It appears that the change of appearance of the sensory retina for the NHP 1- and 24-h thresholds is caused by the physiological reaction of the system to the injured RPE cells. This reaction takes some time to develop, and after that time becomes noticeable as a visible change of appearance. It also follows that it is unlikely that the change of appearance at the 1- or 24-h threshold is thermally induced coagulation of the sensory retina. Thermally induced coagulation of the sensory retina should be visible almost immediately after exposure, which is the case, for instance, in medical photocoagulation treatment of the retina. It is important to distinguish these acutely induced (immediately visible) lesions from changes of retinal appearance at threshold levels determined 1 and 24-h after exposure. Only in the former case is the induced effect immediate thermal coagulation of the RPE as well as of the sensory retina, which requires higher temperatures and higher retinal radiant exposures than the 1- and 24-h injury thresholds which are, however, the more appropriate endpoints for setting safety exposure limits. Also, thresholds that are determined 5 min after exposure are above the thresholds detected at 1 or 24 h after exposure, i.e., a higher exposure level is needed to induce thermal damage that is already visible 5 min after exposure as compared to lesions that become visible at 1 or 24 h after exposure.

4.2 *Small Spot/Spot Size Behavior*

In the previous section we concluded that the underlying damage mechanism for both the *in vivo* NHP 1- and 24-h ophthalmoscopically visible thresholds as well as the *ex vivo* bovine model is likely to be immediate thermal damage of RPE cells. For spot sizes above 80 μm, both models yield almost identical threshold levels. However, for spot diameters less than 80 μm, there is striking deviation of both the computer model and the *ex vivo* bovine model thresholds from the *in vivo* NHP thresholds. In terms of TIE, the NHP thresholds remain almost constant for smaller laser spots, while both the *ex vivo* bovine as well as the computer model continue to decrease with basically a linear spot diameter dependence. At a nominal laser spot diameter of 25 μm, the *ex vivo* bovine and computer model thresholds are a factor of about 3.5 lower than the interpolated NHP threshold. Very similar small spot—spot size behavior is also noted for 532-nm ns-duration thresholds[13] (Fig. 8). As shown by Lund et al.,[9] equivalent small spot/spot size dependence can also be observed for millisecond-duration exposures and ultrashort exposures. The existence of this peculiar small spot behavior for exposure durations that clearly encompass different damage mechanisms (for instance, including bubble formation around melanosomes as seen in nanosecond threshold data, see discussion in Sec. 3.3) leads to the conclusion that the underlying effect is more generic and does not depend on the damage mechanism. Two explanations can be envisaged. (1) The laser spot that is incident on the RPE is enlarged, for instance by scattering, up to about 80 to 100 μm diam, even though the nominal (theoretical) laser spot diameter at the RPE is smaller than that (2) The laser beam at the retina and RPE is not enlarged, but there are factors for the NHP experiments related to the nonvisibility of small lesions. Assuming the retinal spot at the *in vivo* NHP RPE is not enlarged, the lower bovine and computer model thresholds suggest that in the NHP retina, RPE cells should also be damaged at exposure levels lower than those determined experimentally *in vivo*, shown in Fig. 7. In that case, at the small-spot threshold levels determined by the bovine and computer model, the NHP RPE cells would also be damaged. The observed NHP thresholds can be explained when, for some reason, these small diameter RPE lesions in the NHP eye do not produce the necessary change of optical appearance that is necessary to be detected as ophthalmoscopically visible lesions, and "superthreshold" exposure levels are needed to produce lesions that are ophthalmoscopically visible. This could be due to two reasons.

- A small diameter RPE lesion at threshold for RPE damage might not invoke the systemic response that leads to a change of optical appearance of the sensory retina (i.e., RPE damage is present, but the systemic response by the sensory retina seen for larger RPE lesions does not occur). If this explanation were true, the question would remain whether the lesion at RPE damage threshold would be a significant lesion in terms of having an effect on vision. There are reports that dead RPE cells do not necessarily lead to damage of the

associated photoreceptors, but are replaced by neighboring RPE cells sliding into place.[20]

• A systemic response *does* occur in the sensory retina at the RPE damage threshold level, but the optical change of the sensory retina is only noticeable when it has a minimum diameter, i.e., small RPE lesions might induce small diameter systemic responses in the sensory retina, but they are too small to be detected ophthalmoscopically, for instance, due to lack of contrast.

In both bulleted cases in (2), the laser energy per pulse needs to be correspondingly higher to produce a "superthreshold" RPE lesion that produces a systemic response that is ophthalmoscopically visible. For thermally induced lesions, it is tempting to envisage this superthreshold condition as thermal bleeding, i.e., thermal conduction leading to a lesion that is larger than the laser spot on the RPE. However, this can be ruled out by thermal modeling: one can compare the predicted damage threshold for a laser spot with a diameter of 100 μm to cases where the laser spot diameter is smaller than 100 μm but the minimal lesion diameter is set to 100 μm. For pulse durations of about 100 ms, the predicted thresholds for smaller laser beams in terms of energy (TIE) would be equal to the threshold for a 100-μm laser spot diameter, in line with the experimental observations. However, the shorter the pulse duration gets, the more energy is needed for a smaller laser spot diameter to induce a 100-μm lesion, as compared to the threshold for a 100-μm laser spot, which contradicts the experimental observation that the threshold in the small spot regime is a constant energy value. Also, the calculated temperatures in the center of the laser spot would reach unrealistic values; for instance, to induce a 100-μm lesion for a 25-μm laser spot and a pulse duration of 1 ms, the temperature in the center of the laser spot would reach almost 4000 °C. Further, this spot size behavior is also seen for 5-ns exposure durations where the damage mechanism at threshold appears to be bubble formation around the melanosomes in the RPE. For this damage mechanism, it is physically impossible to create the temperature rise necessary for bubble induction in an RPE region significantly larger than the actual region that is exposed to laser radiation, and at the same time exhibit thresholds for smaller diameters that are not higher than the threshold for an 80-μm spot. The same arguments also lead to falsification of the hypothesis that superthreshold levels are needed to induce thermal damage of the sensory retina by conduction from the heated RPE. When *thermal* superthreshold effects can be ruled out, since they cannot explain the small spot/spot size thresholds for short pulses, it is still possible that the superthreshold exposures somehow lead to a *nonthermally* induced amplification of the response of the system as compared to exposure at RPE damage threshold levels. However, the effect would have to produce the observed constant energy thresholds in the NHP model (i.e., equal energy thresholds independent of the spot size for spot sizes less than about 80 to 100 μm) for pulse durations between femtoseconds and seconds. While this possibility cannot be ruled out, it appears somewhat unlikely that such a nonthermal superthreshold effect could produce a constant energy threshold for such a wide range of pulse durations encompassing different damage mechanisms.

In summary, these arguments indicate that explanation number (2) is somewhat unlikely. Consequently, explanation number (1), an increase of the laser beam diameter on its path to the RPE, is further discussed. The obvious reasons for an increase of the laser beam profile are scattering and/or ocular aberration, i.e., wavefront distortion. Aberration is small for small laser beam diameters at the cornea. Forward scattering in the preretinal media has been given as a reason for the current value of the minimal angular subtense for the apparent source in laser safety[21] of 1.5 mrad, which is equivalent to a retinal image diameter of 25 μm, while the diffraction-limited laser spot diameter for a perfect optical system would rather be in the range of 6 μm. However, if preretinal scatter can induce an increase of the retinal image of up to 80 to 100 μm, it should hamper vision, which is not the experience we have as humans. It should be noted that the eye of an anesthetized NHP is held open for exposure, which leads to the possibility of corneal dehydration and an increase in scatter. As an alternative to preretinal scattering, we offer *intraretinal* scatter as a new explanation of the small spot/spot size behavior in the visible wavelength range. Layers in the sensory retina—particularly the uppermost layer, the nerve fiber layer (NFL)—could induce scattering of optical radiation, which increases the diameter of a minimal laser beam incident on the NFL to a diameter of 80 to 100 μm at the RPE, at least in the parafoveal region where the distance between the NFL and the RPE is about 200 to 300 μm. This possibility is supported by images obtained in optical coherence tomography (OCT), where the back-reflection signal of the NFL is relatively strong, even for the usual OCT wavelength of 800 nm. Unterhuber, Považay, and Bizheva[22] compared a number of wavelengths and noted that no signal from the RPE could be detected for the blue 475-nm wavelength, and only a very weak signal for the red 605-nm wavelength. For setting exposure limits, however, it is important to note that the NFL is pushed aside in the foveal pit to increase visual acuity there. The OCT backscatter signal from the sensory retina is minimal in the foveal region, which also ties together with our experience that we have high visual acuity in the fovea only and low acuity vision outside of the foveal region. Therefore, if the explanation of intraretinal scatter holds true, it is to be expected that in the foveal region, a minimal laser beam (25 μm diam for instance) is not significantly increased in diameter due to scattering, and it might well be that for direct exposure of the fovea, the damage thresholds are lower than the ones determined experimentally for the NHP outside of the fovea.

We note that for spot diameters less than 20 μm, the computer model data shown in Fig. 5 as retinal radiant exposure predict a small spot dependence that is steeper than the dependence for spots larger than 20 μm. This is due to the setting of the "minimal visible lesion" in the computer model to a value of 20 μm and the finite grid size of the model. The effect can best be seen for short pulse durations of, for instance, 10 μs where there should be no spot size dependence, i.e., the curve should be horizontal for all spot sizes. However, for the smallest spot size, the threshold is higher. This is not only seen in the computer model data, but can also be discerned for the 23-μm bovine data, which is well fitted by the computer model data (Fig. 5). For the experimental data, the

effect is related to the finite size of an RPE cell, which would be the smallest unit that can be determined to be damaged based on our endpoint, as well as to some likelihood that the 23-μm laser spot is incident not only on one cell (which is of the order of this minimal spot diameter) but on, for instance, three cells, which increases the injury threshold.

4.3 *General Spot Size Dependence*

The thermal model and the *ex vivo* bovine threshold data show a previously unknown variation of the spot size dependence for different pulse duration. When expressed as retinal radiant exposure values, the breakpoint between the D^{-1} threshold dependence and the constant threshold region for larger spots is not constant—as currently implied by the MPEs—but shifts to smaller diameters for shorter pulses. The breakpoint is in the region of 100 mrad (1.7 mm) only for pulse durations longer than 1 s. For pulse durations of less than approximately 100 μs, there is no detectable spot size dependence, i.e., the damage threshold is a constant retinal radiant exposure value, independent of the actual laser spot size (with the exception of spot sizes of the order of the minimal visible lesion). This apparent dependence of the breakpoint on pulse duration can be explained based on thermal diffusion. Thermal diffusivity is a characteristic parameter that can be understood as the speed at which heat diffuses through a medium, or by which a temperature difference travels. The thermal diffusivity D_{th} is defined as the ratio of thermal conductivity over the specific heat and the density of the material, and thus has the units of cm^2/s. Within a time t, a "heat wave" travels approximately a distance of about $2\sqrt{(tD_{\mathrm{th}})}$. This speed is also relevant for the radial cooling of the laser spot. As the heat wave travels in radial direction away from the rim of the disk that is heated by the laser spot, it heats the surrounding nonirradiated region. Due to this heat flow, the irradiated area is cooled, so that the zone that is affected by this cooling action (a negative heat wave, i.e., a cooling wave) travels inward from the rim of the laser spot toward the center of the laser spot. As long as the cooling front does not reach the center of the laser beam, the center of the laser spot remains unaffected by the radial cooling action, and therefore the temperature of the center is independent of the size of the laser spot. Although the Arrhenius damage integral adds up over the full duration where the tissue temperature is elevated, due to the strong nonlinearity of the Arrhenius integral with temperature, the main contribution to the damage integral comes from the higher temperatures during the exposure. Thus, for exposure duration ranges from ms to s, the characteristic time for thermally induced damage is, in first approximation, the laser pulse duration. It follows that the breakpoint characterizes the retinal spot radius (approximately) equal to the thermal diffusion distance for the respective pulse duration. If the spot is larger than this characteristic diameter, the center is not affected by radial cooling and is just given by the local retinal radiant exposure or irradiance, independent of the actual diameter of the spot. If the spot is smaller than this characteristic diameter, the center is affected by cooling, which leads to a lower temperature and to an increase of the threshold in relation to the case where there is no cooling. The smaller the spot, the earlier during the pulse duration the center is affected (cooled) radially, which results in the D^{-1} dependence. (Note, however, that we did not find a simple line of reasoning based on the time-temperature history that would explain or predict the strict D^{-1} dependence, as the Arrhenius integral is highly nonlinear with temperature). We do not believe that axial heat conduction plays a role in the D^{-1} dependence, since axial heat conduction is independent of the laser spot size. The calculated maximum temperature rise for the case of a pulse duration of 100 ms is depicted as radial profiles in Fig. 10 for a range of spot diameters between 100 and 1600 μm for a radiant exposure value equal to the threshold for the 1600-μm spot. For spot sizes above about 800 μm, the central temperature is independent of the spot diameter. This is also approximately the diameter where the horizontal part of the threshold curve for a pulse duration of 100 ms plotted in Fig. 5 commences.

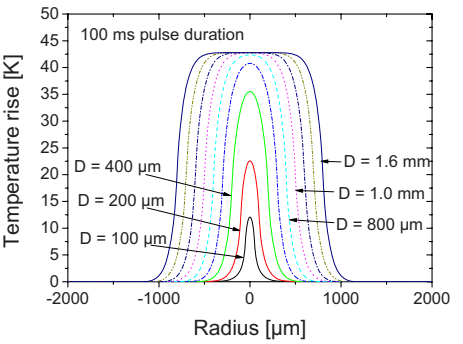

Fig. 10 Calculated radial temperature increase profiles for a range of spot diameters in 200-μm steps starting at 200 μm, plus the curve for a diameter of 100 μm.

4.4 *Time Dependence*

The threshold data can also be plotted as a function of exposure duration for the range of retinal spot sizes to study their time dependence. The time dependence of the spot size dependence breakpoint also results in a variation of time dependence for the different retinal spot sizes currently not reflected in the MPEs. For a diameter of 23 μm, the slope in a log-log scaled time dependence is somewhat steeper than the value of 0.75 currently defined by the MPEs; it equals 0.9 for pulse durations longer than about 1 ms. For shorter exposure durations, the time dependence becomes shallower and, according to the thermal model, becomes zero (i.e., no time dependence) for pulse durations of less than about 10 μs, also referred to as the thermal confinement region. The larger the spot size becomes, the more the region of shallower time dependence extends to longer times, so that for a spot size diameter of 2 mm, according to the model, the time dependence slope in log-log scale becomes 0.4. For exposure durations of less than about 0.1 ms, all the curves (except the one for 23 μm, which is for Gaussian profile and close to the minimal visible lesion dimension) for the different spot sizes merge as they approach the thermal confinement region. Regarding the shallower time dependence for large spots, it can be noted that this is somewhat reminiscent of the time dependence of the MPEs for thermal corneal and skin damage, which is $t^{0.25}$. After all, these corneal and skin MPEs are based on threshold studies that used image diameters in the order of millimeters, which would also exhibit a shallower time dependence than image

sizes of less than 1 mm, relevant for retinal laser exposure. The thermal damage model predicts that under thermal confinement conditions of a homogeneous medium, the thresholds in terms of energy per pulse (or radiant exposure per pulse) would no longer depend on the exposure duration. However, as shown in Sec. 3.3, for exposure durations of less than about 10 μs, bubble-induced damage thresholds become lower than thermal damage thresholds, and the thermal damage model is no longer applicable.

4.5 *Limitation of the Models*

For longer exposure durations in the seconds time regime, the bovine and computer models are limited by heat flow issues, because they do not include blood flow. They also do not model photochemically induced damage at wavelengths in the blue and green region, which for exposure durations in the multisecond range might have lower thresholds than thermally induced injuries. For pulse durations shorter than about 10 μs, the application of the computer model to model thermal damage is limited, since bubble formation and effects of ultrashort pulse exposure cannot be modeled.

5 Conclusions and Summary

As shown in Fig. 5, the computer model can predict *ex vivo* bovine thresholds for 532-nm laser exposure, within the covered pulse duration range of 100 μs to 2 s and retinal spot sizes between 23 μm and 2 mm, very well. Both models, *ex vivo* bovine and computer, agree well with 514-nm *in vivo* threshold spot size dependence data for 1-s exposure duration[16] as well as new 100-ms exposure duration data.[9] The two available *in vivo* datasets for the red wavelength range[17,18] differ by at least a factor of 2 when compared to each other. However, the relative retinal spot size behavior of these datasets is predicted well by the *ex vivo* bovine threshold data and the computer model. This is also the case for xenon lamp threshold data for exposure of NHP retina *in vivo*.[18] It can be concluded that the thermal damage computer model and the *ex vivo* bovine model, for exposure durations between 10 μs and 2 s, for all retinal spot sizes, can be a valuable tool for the absolute prediction of nonhuman primate and human threshold levels.

The advantages of the bovine explant *ex vivo* model compared to *in vivo* NHP models is that precise dosimetry of the energy incident on the retina as well as the beam profile is possible, as well as a stable sample and no influence of corneal clouding or aberrations of the eye. Due to availability and cost, an experimental series that covers two parameters, exposure duration and spot size, over considerable ranges, is not practical with NHP models. Since the computer model is validated against NHP *in vivo* data as well as *ex vivo* explant data, in the future, parameter studies and safety analysis can be conducted by application of the computer model. This is particularly relevant for irregular multiple pulses or scanned retinal exposure for which the current laser safety standards do not provide appropriate, or provide over-restrictive, evaluation methods.

For small spot sizes, the differences between the explant *ex vivo* and computer model threshold data and *in vivo* NHP data provide some insight on possible reasons for the spot size dependence for small spots. Intraretinal scatter is offered as an explanation of the observed small spot/spot size behavior. The safety factor of 10 (which is often incorrectly cited as a general safety factor for MPEs) applies to minimal images when determined with NHP studies only, and is therefore prudent, since the actual threshold for RPE damage might be a factor of 3 lower than the values reported in *in vivo* studies. A safety factor of 3 is found for extended sources in the millisecond time regime, which is sufficient, since thresholds can be determined more accurately. The comparison of threshold data for the *ex vivo* bovine and the *in vivo* NHP models leads to the conclusion that also for the NHP model, the underlying damage mechanism at thresholds detected 1 or 24 h after exposure is likely to be immediate RPE cell damage, not thermal coagulation of the sensory retina.

The *ex vivo* bovine and computer model data show previously unappreciated spot size dependence, where the breakpoint between the linear dependence on spot diameter and the region where the retinal threshold no longer depends on spot size, but depends on the pulse duration. This dependence is supported by an analysis of the collected body of *in vivo* data relating the injury threshold to the retinal spot size.[9] The breakpoint could be adopted as a basis for a time dependent α_{max} in the MPEs to reduce unnecessarily large safety factors, increasing the MPEs for large sources and pulses in the microsecond and millisecond regime by up to a factor of 20.

Acknowledgments

The authors gratefully acknowledge the help and support of the following individuals: David Sliney (U. S. Army Center of Health Promotion and Medicine, Baltimore) and Bruce Stuck (U. S. Army Research Detachment, San Antonio) for frequent and fruitful discussions; Boris Považay of Cardiff University for information provided on high resolution OCT; Paul Kennedy (U. S. Air Force Research Lab, San Antonio) for help in the initial phases of realizing the Thompson-Gerstman model; Donna Clarkson (Northrop Grumman, San Antonio) for preparing histological micrographs; Clemens Alt (Wellman Center for Photomedicine, Harvard Medical School) for demonstrating the *ex vivo* sample preparation method; and Astrid Hrdina (Austrian Research Centers, Toxicology Department) for help with dissecting the cow eyes.

References

1. ICNIRP, "Guidelines on limits for laser radiation of wavelengths between 180 nm and 1,000 μm," *Health Phys.* **71**, 804–819 (1996).
2. ICNIRP, "Revision of guidelines on limits for laser radiation of wavelengths between 400 nm and 1.4 μm," *Health Phys.* **79**, 431–440 (2000).
3. International Electrotechnical Commission, "IEC 60825-1 Safety of laser products-part 1: equipment classification and, requirements," Ed. 2.0, IEC, Geneva (2007).
4. International Electrotechnical Commission, "IEC TR 60825-14 Safety of laser products-part 14: a users's guide," IEC, Geneva (2004).
5. American National Standards institute, "American National Standard for the safe use of lasers, Z136.1-2007," Laser Institute of America, Orlando FL (2007).
6. R. Henderson and K. Schulmeister, *Laser Safety*, Taylor and Francis Group, New York (2004).
7. A. N. Takata, L. Goldfinch, J. K. Hinds, L. P. Kuan, N. Thomopoulis, and A. Weigandt, "Thermal model of laser-induced eye damage," IIT Research Institute Report for Aerospace Medical Division, Chicago, IL (1974).
8. C. R. Thompson, B. S. Gerstman, S. L. Jacques, and M. E. Rogers,

"Melanin granule model for laser-induced thermal damage in the retina," *Bull. Math. Biol.* **58**, 513–553 (1996).
9. D. J. Lund, P. Edsall, B. E. Stuck, and K. Schulmeister, "Variation of laser-induced retinal injury thresholds with retinal irradiated area: 0.1 s duration, 514 nm exposures," *J. Biomed. Opt.* **12**, 024023 (2007).
10. D. H. Sliney, J. Mellerio, V. P. Gabel, and K. Schulmeister, "What is the meaning of threshold in laser injury experiments? Implications for human exposure limits," *Health Phys.* **82**, 335–347 (2002).
11. B. J. Lund, "Computer model to investigate the effect of eye movements on retinal heating during long-duration fixation on a laser source," *J. Biomed. Opt.* **9**, 1093–1102 (2004).
12. A. J. Welch and G. D. Polhamus, "Measurement and prediction of thermal injury to the retina of the Rhesus monkey," *IEEE Trans. Biomed. Eng.* **BME-31**, 1471 (1984).
13. J. A. Zuclich, D. J. Lund, P. R. Edsall, R. C. Hollins, P. A. Smith, B. E. Stuck, L. N. McLin, and S. Till, "Variation of laser-induced retinal damage threshold with retinal image size," *J. Laser Appl.* **12**, 74–80 (2000).
14. G. Schüle, M. Rumohr, G. Hütmann, and R. Brinkmann, "RPE damage thresholds and mechanisms for laser exposure in the microsecond to millisecond time regimen," *Invest. Ophthalmol. Visual Sci.* **46**, 714–719 (2005).
15. H. Lee, C. Alt, C. M. Pitsillides, and C. P. Lin, "Optical detection of intracellular cavitation during selective laser targeting of the retinal pigment epithelium: dependence of cell death mechanism on pulse duration," *J. Biomed. Opt.* **12**, 064034 (2007).
16. E. S. Beatrice and G. D. Frisch, "Retinal laser damage thresholds as a function of the image diameter," *Arch. Environ. Health* **27**, 322–326 (1973).
17. W. T. Ham Jr., W. T. Geeraets, H. A. Mueller, R. C. Williams, A. M. Clarke, and S. F. Cleary, "Retinal burn thresholds for the helium-neon laser in the rhesus monkey," *Arch. Ophthalmol. (Chicago)* **84**, 797–809 (1970).
18. R. G. Allen, W. R. Bruce, K. R. Kay, L. K. Morrison, R. A. Neish, C. A. Neish, C. A. Polaski, and R. A. Richards, "Research on ocular effects produced by thermal radiation," Final Report AF41(609)-3099, Brooks AF Base, TX (1967).
19. E. F. Maher, "Transmission and absorption coefficients for ocular media of the rhesus monkey," USAF School of Aerospace Medicine Report SAM-TR-78-32, Brooks AFB, TX (1978).
20. C. Alt, C. Framme, S. Schnell, R. Brinkmann, and C. P. Lin, "Selective targeting of the retinal pigment epithelium using an acousto-optic laser scanner," *J. Biomed. Opt.* **10**, 064014 (2005).
21. D. H. Sliney and M. Wolbarsht, *Safety with Lasers and Other Optical Sources*, Plenum Publishing Corp., New York, (1980).
22. A. Unterhuber, B. Považay, and K. Bizheva, "Advances in broad bandwidth light sources for ultrahigh resolution optical coherence tomography," *Phys. Med. Biol.* **49**, 1235–1246 (2004).